

Stimulated Raman scattering cascade spanning the wavelength range of 523 to 1750 nm using a graded-index multimode optical fiber

Hamed Pourbeyram

*Department of Electrical Engineering and Computer Science,
University of Wisconsin-Milwaukee, Milwaukee, WI 53211, USA*

Govind P. Agrawal

The Institute of Optics, University of Rochester, Rochester, NY 14627, USA

Arash Mafi

*Department of Electrical Engineering and Computer Science,
University of Wisconsin-Milwaukee, Milwaukee, WI 53211, USA.**

(Dated: 17 April 2013)

We report on the generation of a Raman cascade spanning the wavelength range of 523 to 1750 nm wavelength range, in a standard telecommunication graded-index multimode optical fiber. Despite the highly multimode nature of the pump, the Raman peaks are generated in specific modes of the fiber, confirming substantial beam cleanup during the stimulated Raman scattering process.

PACS numbers: 42.65.-k, 42.81.Ht, 42.65.Dr

Stimulated Raman scattering (SRS) is a well-known nonlinear process with numerous applications including optical amplifiers, tunable lasers, spectroscopy, meteorology, and optical coherence tomography. SRS was first observed in silica glass fibers in 1972 by Stolen et al.¹. They used a frequency-doubled, pulsed, Nd:YAG laser operating at the 532 nm wavelength to pump a single-mode optical fiber and observed Stokes emission at 545 nm. Since then, several groups have reported the observation of SRS in optical fibers using various configurations²⁻⁵. Cohen and Lin² generated 6 cascaded Raman peaks in a silica fiber, pumped by a mode-locked, Q-switched, Nd:YAG laser operating at 1064 nm. Rosman³ observed 15 orders of cascaded Raman peaks by pumping a silica fiber at 532 nm with a frequency-doubled Nd:YAG laser. Other configurations involving unconventional fibers have been used for extreme Raman-comb generation. For example, Couny et al.⁵ demonstrated the generation of a Raman comb spanning wavelengths from 325 nm to 2300 nm in a 1m-long hydrogen-filled hollow-core photonic crystal fiber.

In this article, we report on the generation of new wavelengths, mediated by the SRS process, in a standard graded-index multimode fiber (GIMF). The GIMF is pumped at a wavelength of 523 nm, and a cascade of optical-frequency Raman peaks is generated on the Stokes side of the pump. At high power levels the measured spectrum extends up to 1750 nm, which is the upper detection limit of our optical spectrum analyzer (OSA). The generation of such a wide wavelength range, extending from 523 to 1750 nm, using a large-core telecommunication-grade multimode fiber distinguishes our results from those carried out in small-core or highly customized optical fibers.

Multimode optical fibers are easy to handle and are also easy to align to external sources; however, their large core diameter is perceived as undesirable for nonlinear

applications. Despite a lower effective nonlinearity associated with a larger core of conventional multimode fibers, the multimode nature of these fibers can play an important role in some nonlinear applications. In particular, the presence of multiple propagating modes with different dispersive properties results in expanded phase-matching opportunities for the generation of four-wave mixing (FWM) signals in optical fibers^{4,6-8}. The GIMF used in our experiments has two desirable properties that make it particularly suitable for SRS generation. First, because the effective modal area of each mode in the GIMF scales only as square root of the core area, the effective nonlinearity of some propagating modes is comparable with conventional single-mode fibers⁹. Second, a relatively high GeO₂ content in the core of the standard telecommunication GIMF used in our experiments results in a higher peak Raman gain coefficient compared with silica-core fibers¹⁰.

The pump used in our experiment is a frequency-doubled, Q-switched, Nd:YLF laser operating at 523 nm wavelength, and its 8-ns duration pulses are coupled to the input tip of the fiber using a microscope objective. The laser beam is not diffraction-limited, and many modes in the fiber are excited simultaneously. The GIMF is a 1-km long standard, 50/125- μm , bare fiber (Corning ClearCurve OM2). The output spectrum is measured using a CCS200 spectrometer (from Thorlabs) operating in the range of 200–1000 nm and a MS9740A OSA (from Anritsu) covering the 600–1750 nm wavelength range. We measured the energy of input pulses required for reaching the Raman threshold immediately after coupling into the fiber (less than 1-meter of propagation inside the GIMF) to be 20.9 μJ ; we estimate the peak power to be about 2.5 kW. The pulse energy decreased to about 0.515 μJ after 1-km of propagation, which is consistent with the expected attenuation of about 16 dB/km at the pump wavelength. The measured thresh-

old power for the first Raman peak (P_0^{cr}) is consistent with $g_R P_0^{cr} L_{\text{eff}} \approx 16 A_{\text{eff}}^6$ using the effective length of $L_{\text{eff}} = 270$ m (considering the 16 dB/km attenuation), $g_R \approx 2.9 \times 10^{-13}$ m/W (at 523 nm wavelength and considering the GeO₂ doping), and an effective area of $A_{\text{eff}} = \pi \times (62.5 \mu\text{m})^2$ (considering the heavily multimode and overfilling nature of the pump).

The sequential generation of cascaded Raman peaks is initiated by the pump at 523 nm. As the pump power is increased, the first Stokes line extracts power from the pump until it becomes strong enough to seed the generation of next Stokes line. This process continues and more and more Raman peaks are generated with increasing pump power. The 20 cascaded peaks shown in Fig. 1(a) extend from 523 nm to just above 1000 nm in wavelength. The estimated input peak power of our pump pulses is 22 kW for this figure.

As the pump power is further increased, even more cascaded Raman peaks appear beyond the 1000 nm wavelength range of our spectrometer. Figure 1(b) shows the spectrum measured with the Anritsu OSA in the range of 900–1750 nm at the maximum pump power level (just below the burning threshold of fiber’s input tip). We stress that the two plots in Figs. 1(a) and 1(b) should not be compared directly because they correspond to different power levels and employ different vertical scales. The spectral dip at around 1300 nm and the broad peak beyond 1400 nm are two notable features in this infrared range. The appearance of the spectral dip centered at the 1320-nm wavelength is related to a reduction in the SRS gain occurring near the zero-dispersion-wavelength (ZDW) of the GIMF, where the SRS gain is suppressed due to a near-perfect phase-matching of the FWM process^{11,12}. The dip at 1320 nm can be seen more clearly in Fig. 2, where we plot the data in Fig. 1(b) on a logarithmic power scale.

In our opinion, the broad peak centered at 1600 nm results from the onset of modulation instability in the presence of anomalous dispersion. The resulting short pulses can experience Raman-induced spectral shifts as well as collision-based spectral broadening, resulting in a broad supercontinuum-like feature^{13,14}. The generation of the longer wavelengths beyond the ZDW is a very complex phenomenon and is heavily influenced by parametric processes. Even in the absence of perfect phase matching, FWM can seed higher-order Raman waves that are subsequently amplified through SRS^{15,16}.

The presence of efficient FWM phase-matching opportunities in the GIMF impacts considerably the generation of the cascaded Raman peaks. Figure 3 shows the spectrometer data in the frequency domain, by plotting on the horizontal axis the frequency shift of the Raman comb relative to the pump frequency, and power on a logarithmic scale on the vertical axis. Equal spacing of various peaks on the Stokes side is expected for a cascaded Raman process. However, the presence of FWM frequencies on the anti-Stokes side of the pump is the most notable feature in this figure. The phase-matched frequency

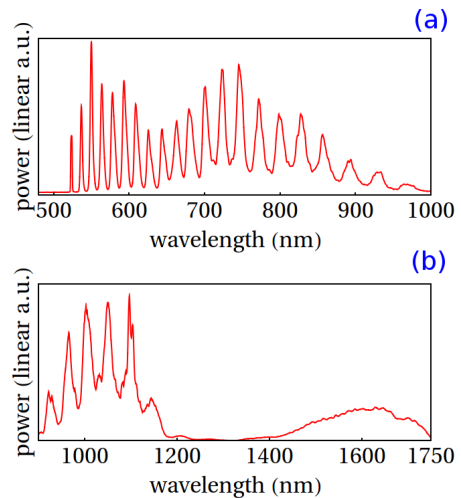


FIG. 1: (a) Cascaded Raman peaks measured with the spectrometer. (b) Spectrum measured by the OSA when pump power is increased to just below the burning threshold of fiber’s tip; the spectral dip at around 1300 nm and the broad peak beyond 1400 nm are two notable features in this infrared range.

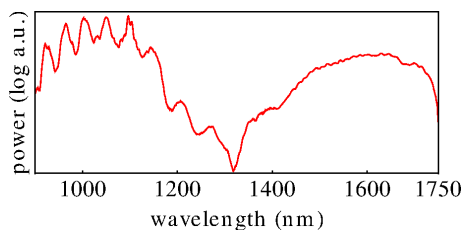


FIG. 2: Same as Fig. 1(b) but data plotted using a logarithmic vertical scale. The input pump power is just below the burning threshold of fiber’s tip.

counterparts of these FWM idlers on the Stokes side can affect the location and amplitude of the cascaded Raman peaks. We observed that the strength of the FWM signal depended on launch conditions, and FWM was absent (or highly suppressed) in some of our measurements. The highly multimode nature of the pump made it very difficult to find the optimum launch position for the generation of the anti-Stokes peaks; we needed to scan the input pump beam over the fiber core to find the point at which the anti-Stokes peaks appeared with considerable power.

In order to explore the effect of FWM on the SRS peaks, we offset the input pump beam by $\approx 15 \mu\text{m}$ from the center of the fiber core. The pump now excites the GIMF modes with different power ratios, resulting in efficient FWM in a different set of phase-matched wavelengths. The result is a shift in the position of the spectral combs. The red and green spectra in Fig. 4 are measured before and after offsetting the pump laser, respectively. The shift seems to be seeded around the third cascaded Raman peak, separated by about 50 THz from

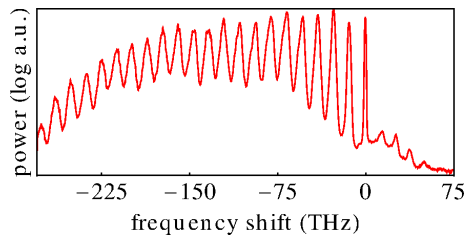


FIG. 3: Cascaded Raman peaks measured with the spectrometer and plotted using frequency shift on the horizontal axis. Notice the presence of FWM peaks on the anti-Stokes side.

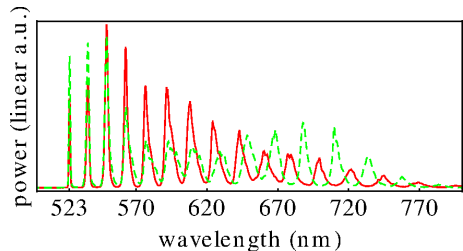


FIG. 4: SRS spectra measured before (red solid line) and after (dashed green line) a slight offset of the pump beam from the fiber center. Shift of Raman peaks is caused by different FWM conditions caused by excitation of different fiber modes.

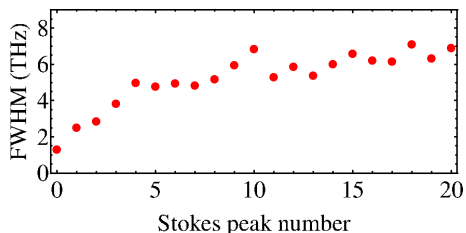


FIG. 5: The FWHM spectral width of the Raman peaks from Figs. 1(a) and 3 are plotted as a function of the Stokes peak number. The Stokes peak numbers 0 and 1 correspond to the pump and the first order Raman peak, respectively.

the pump frequency, which is also consistent with the location of a FWM peak in Fig. 3. We observed that the shift is reversed if the input pump beam is aligned back with the center of the fiber core. Similar observations of the effect of the FWM processes on shifting the SRS spectrum have been reported by Sharma et al.¹⁷; they have shown that the cascaded Raman peaks can shift depending on which modes are excited by the pump laser.

In Fig. 5, we plot the spectral width (full width at half maximum or FWHM) of the Raman peaks from Figs. 1(a) and 3 as a function of the Stokes peak number. The numbers 0 and 1 correspond to the pump and the first order Raman peak, respectively. Ref.¹⁹ predicted that spectral width of each Raman peak is nearly twice that of the preceding order because of the broad bandwidth of the Raman gain in fused silica. The measured FWHM spectral widths of the pump and the first or-

der Raman peak are 1.30 THz and 2.51 THz, respectively. According to Refs.^{18,19}, the spectral bandwidth of the Raman peak under certain conditions is nearly twice that of the pump. However, their analysis makes the undepleted-pump approximation and assumes an unchirped Gaussian profile for the pump pulse, neither of which apply to our experiment. Moreover, the noisy nature of the SRS peaks makes the analysis of Refs.^{18,19} even less applicable to the spectrum of higher-order Raman peaks. In our case, the bandwidths of higher-order Raman peaks show an increasing trend as a function of their Stokes peak numbers.

We also measured the transverse intensity profile of the output beam by a CCD camera using several bandpass color filters with a FWHM spectral bandwidth of about 10 nm. The results are shown in Fig. 6. The profile in Fig. 6(a) is measured without a color filter, and the interference of multiple modes can be clearly observed as a speckle pattern. When a color filter centered at 610 nm is placed in front of the beam Fig. 6(b), we observe a narrow round spot that appears to correspond to the spatial profile of the fundamental LG_{00} mode of our GIMF. We note that LG stands for Laguerre-Gaussian which are the eigenmodes of the GIMF under the weak-guidance approximation. The LG_{nm} modes can be related to the familiar notation of the $LP_{m,n+1}$ modes commonly used for step-index fibers. A donut-shape spot Fig. 6(c) is observed when a color filter centered at 700 nm is placed in front of the beam; the shape and the size of the beam makes us believe that it corresponds to the LG_{01} mode of our fiber. We note that in practice, the two fold degeneracy of the LG_{01} mode is slightly broken to orthogonal double-lobed spatial profiles of Hermite-Gaussian modes²⁰ due to birefringence (similar to the two polarization of the LP_{01} modes). The donut shape in our measurement arises when both double-lobed spatial profiles are present simultaneously, primarily due to the large bandwidth (10 nm) of the color filter used for imaging the modes resulting from the incoherent combination of the orthogonal double-lobed spatial profiles.

Spatial beam profiles corresponding to higher-order fiber modes were also seen in our experiment. As two examples, images (d) and (e) of Fig. 6 show profiles corresponding to the LG_{10} and LG_{20} modes. They were obtained by using optical filters with a 10-nm passband centered at 770 nm and 890 nm wavelengths, respectively. The most notable feature we want to stress is that a GIMF can be used as a device that not only shifts the pump wavelength toward the red side through SRS but also performs the beam cleanup owing to the fact that different-order Raman peaks generally propagate in different modes of the fiber. The main reason for the Raman beam cleanup is that the lower order modes generally have a larger Raman gain because of their greater overlap with the higher concentration of GeO_2 near the center of the GIMF core¹⁰. A detailed analysis of SRS-induced beam cleanup in graded-index multimode optical fibers can be found in Ref.²¹. Chiang reported similar re-

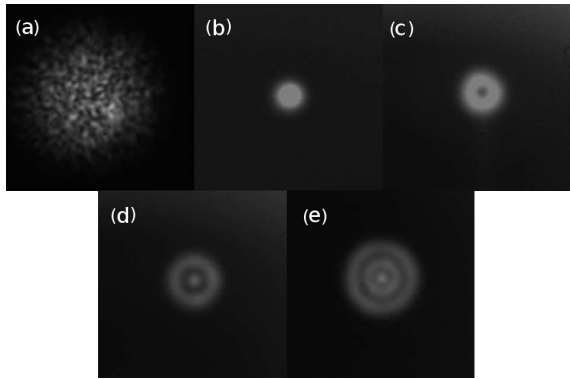


FIG. 6: Measured spatial profiles using a CCD-based beam profiler. Image (a) is measured with no filters. The other 4 images are obtained using color filters centered at (b) 610 nm, (c) 700 nm, (d) 770 nm, and (e) 890 nm.

sults for higher order SRS combs in a 30-m-long fiber²². However, only LP₀₁ mode (corresponding to LG₀₀ mode here) was observed for a 1-km-long fiber. In our experiments, we observed higher-order modes even for a 1-km-long fiber, and beam cleanup was not at the same level reported in Ref.²².

In conclusion, we have used a standard, telecommunication-grade, graded-index multimode fiber for SRS generation by pumping it at 523 nm with 8-ns pulses. We observe multiple cascaded Raman peaks extending up to 1300 nm. Beyond that wavelength, the

nature of dispersion changes from normal to anomalous because our fiber has its zero-dispersion wavelength near 1320 nm. At higher pump powers, in addition to the multiple cascaded Raman peaks, we observe a single broadband spectral peak, extending from 1350 to 1750 nm. Its origin appears to be related to the formation of solitons through modulation instability, intrapulse raman scattering, as well as collision-based spectral broadening. Such features have been observed in the past for single-mode fibers or few-mode step-index fibers (see, e.g., Mussot et al.²³). Our experiments show that a supercontinuum can also form in a highly multimode telecommunication-grade, graded-index multimode fiber. The multimode nature of the fiber can also be useful from a practical standpoint. For example, we observed that different spectral peaks have spatial patterns that correspond to different fiber modes. This feature can be useful for beam cleanup. Future efforts will focus on extending the spectrum to the infrared region and on stabilizing the frequency and power of individual comb lines for practical applications.

Acknowledgments

A. Mafi acknowledges support from the UWM Research Growth Initiative grant and the Air Force Office of Scientific Research under Grant FA9550-12-1-0329.

* corresponding author.

- ¹ R. H. Stolen, E. P. Ippen, and A. R. Tynes, *Appl. Phys. Lett.* **20**, 62 (1972).
- ² L. G. Cohen and C. Lin, *IEEE J. Quantum Electron.* **QE-14**, 855 (1978).
- ³ G. Rosman, *Opt. Quantum Electron.* **14**, 92 (1982).
- ⁴ V. V. Grigor'yants, V. I. Smirnov, and Y. K. Chamorovskii, *Sov. J. Quantum Electron.* **12** 841 (1982).
- ⁵ F. Couny, F. Benabid, P. J. Roberts, P. S. Light, M. G. Raymer, *Science* **318** 1118 (2007).
- ⁶ G. P. Agrawal, *Nonlinear Fiber Optics*, 5th ed. (Academic Press, 2012).
- ⁷ R. H. Stolen, J. E. Bjorkholm, and A. Ashkin, *Appl. Phys. Lett.* **24**, 308 (1974).
- ⁸ J. Cheng, M. E. V. Pedersen, K. Charan, K. Wang, C. Xu, L. Gruner-Nielsen, and D. Jakobsen, *Appl. Phys. Lett.* **101**, 161106 (2012).
- ⁹ A. Mafi, *J. Lightwave Technol.* **30**, 2803 (2012).
- ¹⁰ A. Polley and S. E. Ralph, *IEEE Photon. Technol. Lett.* **19**, 218 (2007).
- ¹¹ E. Golovchenko, P. V. Mamyshev, A. N. Pilipetskii, E. M. Dianov, *IEEE J. Quantum Electron.* **26**, 1815 (1990).
- ¹² F. Vanholsbeeck, P. Emplit, and S. Coen, "Complete experimental characterization of the influence of parametric four-wave mixing on stimulated Raman gain," *Opt. Lett.*

28, 1960 (2003).

- ¹³ B. H. Chapman, S. V. Popov, R. Taylor, *IEEE Photon. Technol. Lett.* **24** 1325 (2012).
- ¹⁴ J. M. Dudley and J. R. Taylor, *Supercontinuum Generation in Optical Fibers*, 1st ed. (Cambridge University Press, 2010).
- ¹⁵ F. Vanholsbeeck, S. Coen, P. Emplit, C. Martinelli, and T. Sylvestre, *Opt. Lett.* **29**, 998 (2004).
- ¹⁶ T. Sylvestre, H. Maillotte, E. Lantz, and P. Tchofo Dinda, "Raman-assisted parametric frequency conversion in a normally dispersive single-mode fiber," *Opt. Lett.* **24**, 1561 (1999).
- ¹⁷ A. Sharma, M. Dokhanian, Z. Wu, A. Williams, and P. Venkateswarlu, *Opt. Lett.* **19**, 1122 (1994).
- ¹⁸ J. I. Gersten, R. R. Alfano, and M. Belic, *Phys. Rev. A* **21**, 1222 (1980).
- ¹⁹ I. Ilev, H. Kumagai, K. Toyoda, and I. Koprnikov, *Appl. Opt.* **35**, 2548 (1996).
- ²⁰ M. B. Shemirani, W. Mao, R. A. Panicker, and J. M. Kahn, *J. Lightwave Technol.* **27** 1248 (2009).
- ²¹ N. B. Terry, T. G. Alley, and T. H. Russell, *Opt. Express* **15**, 17509 (2007).
- ²² K. S. Chiang, *Opt. Lett.* **17**, 352 (1992).
- ²³ A. Mussot, T. Sylvestre, L. Provino, and H. Maillotte, *Opt. Lett.* **28**, 1820 (2003).